ORIGINAL RESEARCH

Run-Mu-Ling Granules Mitigate Ocular Surface Inflammatory Injury Associated with Dry Eye by Suppressing the NLRP3/GSDMD-Mediated Pyroptosis Pathway

Dan Luo [1],*, Hui-jie Ji [1],*, Xue-qing Yan [1], Zi-meng Wang [1], Liu-jiao Li[2], Li Shi [1], Wei-ping Gao[1], Kai Li[1]

[1]Department of ophthalmology, Affiliated Hospital of Nanjing University of Chinese Medicine, Jiangsu Province Hospital of Chinese Medicine, Nanjing, People's Republic of China; [2]Liuzhou Traditional Chinese Medicine Hospital, Liuzhou, People's Republic of China

*These authors contributed equally to this work

Correspondence: Kai Li; Weiping Gao, Department of Ophthalmology, Affiliated Hospital of Nanjing University of Chinese Medicine, Nanjing, People's Republic of China, Email likai8922@163.com; 260790@njucm.edu.cn

Purpose: Run-Mu-Ling granules (RMLG), a traditional Chinese medicinal formula, are used to treat dry eye (DE); however, the underlying mechanism remains poorly understood. This study aimed to elucidate the potential molecular mechanisms by which RMLG alleviates ocular surface inflammation in DE.

Methods: We established an in-vivo DE rat model and in-vitro human corneal epithelial cell line (HCEC) injury models. Corneal damage severity was evaluated using various tests, including corneal fluorescein staining, tear break-up time, and phenol red tear test. Hematoxylin and eosin staining was used to examine histopathological changes in corneal tissues. Terminal deoxynucleotidyl transferase-mediated dUTP nick-end labeling detected corneal cell damage in rats. Transmission electron microscopy was used to observe the microstructures of corneal tissue. Immunofluorescence and Western blotting analyses were used to assess NLRP3, GSDMD, ASC, caspase-1, IL-18, IL-1β, and TNF-α expression levels in corneal tissues and HCEC. Cell viability was determined using CCK-8 and colony formation assays, and pyroptosis was examined using Annexin V-PI staining.

Results: RMLG significantly improved tear film stability, promoted tear secretion, attenuated corneal tissue damage, enhanced HCEC activity, and suppressed pyroptosis. It also inhibited the activation of the NLRP3/GSDMD signaling pathway in corneal tissues and HCEC, reducing the release of downstream pro-inflammatory cytokines.

Conclusion: This study suggests that NLRP3/GSDMD-mediated pyroptosis plays a crucial role in the pathogenesis of DE and that inhibition of this pathway is a key mechanism by which RMLG alleviates ocular surface inflammation in DE. These findings suggest that RMLG could be a promising therapeutic option for DE, offering new insights into its molecular action and potential clinical application.

Keywords: RMLG, dry eye, corneal damage, inflammation, pyroptosis, traditional Chinese medicine

Introduction

Dry eye (DE) is a complex ocular surface disease characterized by tear film instability, hyperosmolarity, and ocular surface inflammation, which collectively disrupt homeostasis and lead to symptoms such as eye discomfort and visual impairment.[1] As a prevalent chronic ocular surface disease, the incidence of DE rises annually. According to the TFOS DEWS II epidemiology report, the global prevalence of DE ranges from approximately 5% to 50%. In Asia, the prevalence reaches as high as 14.4% to 24.4%, significantly impacting daily life and work and highlighting its status as a global public health concern.[2,3] Various factors, including ocular lesions, systemic diseases, and environmental factors, disrupt ocular surface homeostasis, resulting in DE.[3,4] Currently, tear substitutes, immunomodulators, and corticosteroids are commonly used to

treat DE in clinical practice. However, tear substitutes have a limited duration of action on the ocular surface, whereas immunomodulators require several months to achieve optimal efficacy. Additionally, long-term use of corticosteroid eye drops poses potential risks, such as glaucoma and cataract development, making the management of DE particularly challenging.[5,6]

The pathogenesis of DE is complex, with ocular surface inflammation being a key factor.[7] Innate immune cells recognize pathogens through pattern recognition receptors, triggering inflammatory responses. Inflammasomes integrate pathogens, cells, tissue damage, and exogenous signals,[8] and play a central role in the pathogenesis of almost all chronic inflammation types associated with metabolic, genetic, systemic, and ocular diseases. Studies have implicated activation of the NOD-like receptor pyrin domain-containing protein 3 (NLRP3) inflammasome in DE occurrence and development.[9] Inflammation promotes the expression of NLRP3 and apoptosis-associated speck-like protein containing a caspase recruitment domain, activates caspase-1, and drives pro-inflammatory cytokine interleukin (IL)-1β and IL-18 maturation and release. Concurrently, caspase-1 cleaves gasdermin D (GSDMD) to produce an N-terminal cleavage product (GSDMD-N), leading to pyroptosis through plasma membrane pore formation.[10]

Pyroptosis, a key component of innate immunity, is a form of programmed inflammatory cell death mediated by gasdermin, first discovered in *Salmonella*-induced macrophage death.[11] Based on different activation modes, pyroptosis is divided into three types: classical, non-classical, and the Caspase-3-mediated pyroptosis pathway.[12] All forms lead to GSDMD activation, causing cell membrane rupture and release of IL-18 and IL-1β.[13] Pyroptosis plays a significant role in various eye diseases, such as keratitis, diabetic retinopathy, and age-related macular degeneration.[14–16] Increasing evidence suggests that the GSDMD-mediated pyroptosis pathway is pivotal in the pathogenesis of DE.[17,18] Recently, studies have shown that activation of inflammatory signaling pathways in DE can induce pyroptosis and pro-inflammatory responses in corneal epithelial cells.[19,20] Li et al suggest that oridonin may alleviate ocular surface injury by inhibiting the NLRP3/caspase-1/GSDMD pyroptosis pathway in a DE model.[21] Therefore, targeting the NLRP3/GSDMD-mediated pyroptosis pathway could represent a potential therapeutic strategy for DE.

Traditional Chinese medicine may support DE prevention and treatment because of its multi-target approach and low toxicity.[22–24] Run-Mu-Ling granules (RMLG), prepared by Jiangsu Provincial Hospital of Traditional Chinese Medicine, have shown clinical efficacy in patients with DE by repairing corneal epithelial injury and alleviating symptoms. Some evidence suggests that RMLG inhibits inflammation, reverses corneal epithelial defects, reduces goblet cell dysfunction, and restores tear secretion, thus supporting tear film and ocular surface homeostasis.[25] In animal studies, Son et al demonstrated that the Runmuling formula exerts anti-inflammatory effects by reducing ocular surface injury and inhibiting ocular surface inflammation, effectively treating DE.[26]

The formulations of RMLG used in this study included *Bidens pilosa* L., *Lycium barbarum* L., and *Chrysanthemum × morifolium* (Ramat). Hemsl. A previous pharmacological study by our group indicated that *B. pilosa* extract, the main component of RMLG, is effective in treating androgen-deficient DE in rats by improving aqueous tear quantity, maintaining tear film stability, and inhibiting lacrimal gland inflammation.[27] However, the exact mechanism of action of RMLG in the treatment of DE remains unknown and requires further investigation. Therefore, this study aimed to evaluate the effects of RMLG on ocular surface inflammation in DE in rats and human corneal epithelial cell (HCEC) injury, exploring the key targets, pathways, and potential molecular mechanisms underlying DE pathogenesis and laying the foundation for its clinical application in DE treatment.

Material and Methods
Key Reagents and Chemicals

Scopolamine hydrobromide (Scop) (catalog number JOT-10515) was procured from Pufei De Biotech Co., Ltd. (Chengdu, China). Benzalkonium chloride (BAC) (catalog number 768584) and nigericin (catalog number N849347) were procured from Macklin Biotech Co., Ltd. (Shanghai, China). MCC950 (catalog number S7809), a specific inhibitor of NLRP3 inflammasome activation, was procured from Selleck Co., Ltd. (Houston, TX, USA) and used as a positive control.[28]

The following antibodies were used in this study: Anti-NLRP3 (WL02635), Anti-Cleaved-caspase-1 (WL03450) from Wanlei Biotech Co., Ltd. (Shenyang, China), Anti-ASC (TU283162), Anti-Caspase-1 (T510200F) from Abmart Co., Ltd. (Shanghai, China), and Anti-beta Actin (ab8227), goat anti-rabbit IgG (ab150077), and goat anti-mouse IgG (ab150113) from

Abcam (Cambridge, UK). Anti-GSDMD (66387-1-Ig), anti-TNF-α (60291-1-Ig), anti-IL-1β (66737-1-Ig), and anti-IL-18 (60070-1-Ig) antibodies were procured from Proteintech Group, Inc. (Wuhan, China).

The following kits were used in this study: TUNEL kit, BCA protein concentration determination kit, CCK-8 Kit, cell cycle and apoptosis detection kit from Beyotime Biotech Co., Ltd. (Shanghai, China).

Preparation of RMLG

RMLG was procured from the Affiliated Hospital of Nanjing University of Chinese Medicine and produced by Tianjiang Pharmaceutical Co., Ltd. (Jiangsu, China). It is a traditional Chinese medicinal formula composed of three botanical drugs: *B. pilosa* (Asteraceae), *L. barbarum* (Solanaceae), and *Chrysanthemum × morifolium* (Asteraceae). Plant names were verified using an online database http://mpns.kew.org. Details of the specific botanical drugs are shown in Table 1.

The preparation of RMLG was conducted as follows: first, the botanical drugs weighed in a 3:1:1 ratio (B. *pilosa: L. barbarum: Chrysanthemum × morifolium*). The botanical drugs were crushed appropriately and then decocted three times with 10 times the volume of pure water; the decoction was separated and collected, ethanol was added after cooling and mixed thoroughly, and the supernatant was removed after it was settled and filtered. The ethanol was recovered under reduced pressure and concentrated under a vacuum to achieve an extract solution concentration of 1 g/mL. Excipients (β-cyclodextrin: α-lactose=1:5) were added to the extract, it was mixed well and then spray-dried to form extract powder. Finally, the dry granulation method was used to press the extract powder into granules. The extraction rate of RMLG was 0.143 (1 g of extract was equivalent to 7 g of botanical drug).

Metabolite Analysis of RMLG

The metabolites of RMLG were analyzed using liquid chromatography-tandem mass spectrometry (LC-MS/MS). LC-MS/MS analysis was performed using a SHIMADZU-LC30 ultra-high performance liquid chromatography (UHPLC) system equipped with a Waters ACQUITY UPLC® HSS T3 column (2.1×100 mm, 1.8 μm particle size, Milford, MA, USA). The sample injection volume was set to 6 μL, and the temperature was maintained at 40 °C. The flow rate was set at 0.3 mL/min. The mobile phase consisted of 0.1% formic acid in water (solution A) and 0.1% formic acid in acetonitrile (solution B). The gradient elution program was as follows: 0−2 min, 0% B; 2−6 min, 0%−48% B; 6−10 min, 48%−100% B; 10−12 min, 100% B; 12−12.1 min, 100%−0% B; 12.1−15 min, 0% B.

A Q Exactive Plus mass spectrometer (Thermo Fisher Scientific Inc., Waltham, MA, USA) was used for mass spectrometric analysis. Both positive (+) and negative (-) modes were detected using electrospray ionization (ESI). The mass spectrometer conditions were as follows: spray voltage: 3.8 kv (+) and 3.2 kv (-); capillary temperature: 320 °C; sheath gas flow rate: 30 L/min; auxiliary gas flow rate: 5 L/min; probe heater temp, 350 °C; S-Lens RF level: 50.

Animal Experiments

Animals

Specific pathogen-free grade male Sprague-Dawley rats (weighing 180–220 g) were procured from SiPeiFu Biotech Co., Ltd. (SCXK [Jing] 2019–0010, Beijing, China), and slit-lamp microscopy examination revealed no abnormalities in the anterior segments of the rats. The animals were housed in the Laboratory of Pharmacology, Affiliated Hospital of Nanjing University of Chinese Medicine (SYXK [Su] 2022–0070), where they were maintained in a controlled environment at a room temperature of 23±2 °C and relative humidity of 50±10%, with a 12 h day-night cycle, and free access to food and water. All procedures involving animals complied with the national regulations on the management of experimental animals and

Table 1 Formulation of RMLG

Botanical Name	Traditional Name in Chinese	Medicinal Part	Production Methods
Bidens pilosa L.	Guizhencao	Dry part of the ground	Granules
Lycium barbarum L.	Gouqi	Fruit	Granules
Chrysanthemum × morifolium (Ramat.) Hemsl.	Juhua	Dried flower bud	Granules

were approved by the Animal Ethics Committee of Affiliated Hospital of Nanjing University of Chinese Medicine (Ethical license: 2022DW-39-02).

Animal Model of DE

After a 1 week adaptive feeding period, the animals were randomly divided into two groups: a DE model group (n=40) and a control group (n=10). The rats in the DE model group were subcutaneously injected with a 3 mg/mL solution of Scop at a dose of 0.6 mg/0.2 mL/time, four times a day (8 a.m., 11 a.m., 2 p.m., and 5 p.m.) for 10 d.[29] The success of the model was based on the following characteristics: (i) corneal epithelial cell damage (characterized by increased staining of spots or plaques), (ii) significantly reduced tear break-up time, and (iii) significantly decreased tear secretion.[30] Rats in the control group were injected subcutaneously with an equal volume of saline at the same site.

Drug Administration and Animal Grouping

After 10 d of modeling, the DE model rats were randomly divided into four groups: model group, RMLG low-dose (RMLG-L) group, RMLG high-dose (RMLG-H) group, and NLRP3 inflammasome inhibitor (MCC950) group (n=10 per group). Rats in the Chinese medicine groups received RMLG intragastrically once a day (10 a.m)., and the rats in the positive control group were intraperitoneally injected with MCC950 solution at a dose of 10 mg/kg/d (10 a.m).[31] The dosage of the Chinese medicine group was based on the body surface area of rats and clinical normal crude drug use. The clinical dosage of Run-Mu-Ling decoction is 50 g crude drug/d per person (standard weight 60 kg), which was converted into a dose of 5.25 g crude drug/kg/d for rats; the equivalent RMLG dosage was 0.75 g granule/kg/d. We set the equivalent dose of 0.75 g granule/kg/d as the low dose, and the high dose was equal to twice the low dose, ie, 1.5 g granule/kg/d. Rats in the control and DE model groups received equal volumes of pure water intragastrically. The DE model was maintained by subcutaneous injection of Scop until the end of treatment. After 2 weeks of treatment, the rats were sacrificed using isoflurane asphyxia, and corneal tissues were collected for further experiments. An illustration of the experimental procedure is presented in Figure 1A.

Cell Experiments

Cell Culture and Transfection

The HCECs were procured from Fenghui Biotech Co., Ltd. (Hunan, China). The HCECs were cultured in Dulbecco's modified Eagle medium supplemented with 10% fetal bovine serum and 1% penicillin-streptomycin in a humidified atmosphere with 5% CO_2 at 37 °C. The cells were sub-cultured until they reached the logarithmic growth phase.

NLRP3 was silenced by RNA interference. Specific NLRP3 small interfering RNA (NLRP3-siRNA) and scrambled siRNA negative control (NC-siRNA) were synthesized by Yunzhou Biotech Co., Ltd. (Guangzhou, China). Based on the principle of RNA interference sequence design, the NLRP3-siRNA sequence was designed to target the NLRP3 gene sequence, as follows, Guide: 5'-ACUUUUGUCUCAUAAUUGAA-3'; Passenger: 5'-CAAUUAUGAGACAAAA AGUGC-3'. The NC-siRNA sequence was designed as follows, Guide: 5'-UUUUUGAACAAGUUAAUAGAC-3'; Passenger: 5'-CUAUUAACUUGUUCAAAAAAG-3'. HCECs were transfected with Lipofectamine 2000 according to the manufacturer's instructions, and the silencing effect of NLRP3 was verified by Western blotting.

Cell Viability Assay

In-vitro BAC concentration screening and HCEC activity were determined by Cell Counting Kit-8 (CCK-8). A total of 5×10^3 HCECs were seeded into a 96-well plate during the logarithmic phase and then treated with BAC at concentrations of 0.0005, 0.001, 0.005, 0.01, 0.05, and 0.1% at 37 °C in a 5% CO_2 cell incubator.[32] After 6 h of treatment, following the manufacturer's instructions, 10 μL of CCK-8 was added to each well and incubated at 37 °C for 3 h. The absorbance at 450 nm was recorded using a microplate reader (Allsheng Instruments Co., Ltd., Hangzhou, China), and we screened the half-maximal inhibitory concentration as the cell modeling concentration.
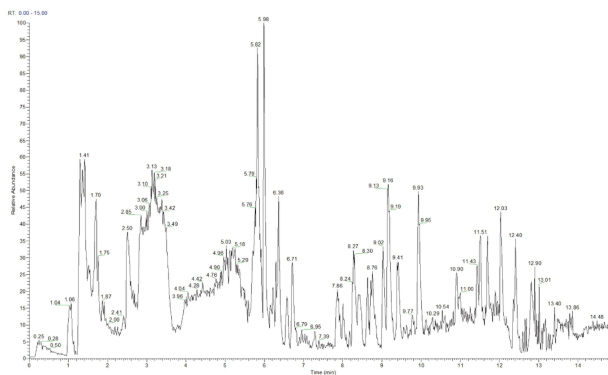
Drug Administration and Cell Grouping

Twenty male SD rats were randomly divided into the blank and RMLG groups (n=10 each). Rats in the RMLG group were intragastrically administered RMLG (0.75g granule/kg/d) twice daily for 5 days, whereas rats in the blank group received
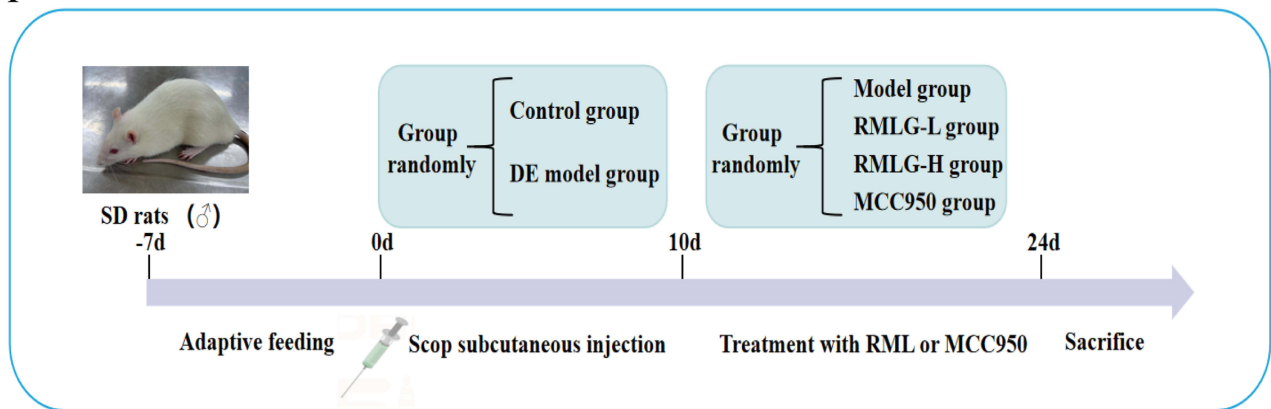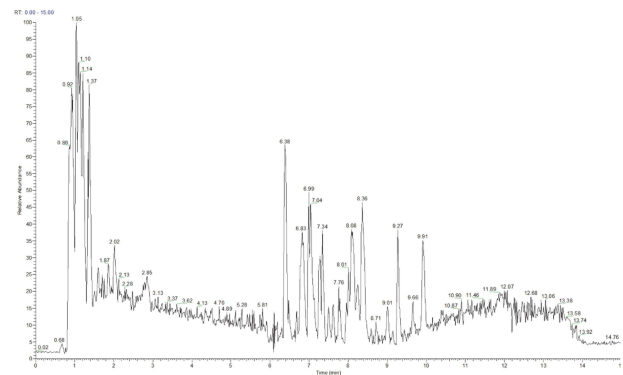
Figure I Experimental protocol for RMLG studies in DE rats and metabolite analysis of RMLG. (**A**) Subcutaneous injection of scopolamine (Scop) for 10 d was used to create a DE model in rats after 7 d of adaptive feeding, RMLG was administered by oral gavage, and the NLRP3 inhibitor (MCC950) was administered by intraperitoneal injection from days 11–24. Animals were sacrificed after 2 weeks of treatment, and the correlation index was determined. (**B**) Base peak map of RMLG in positive ion model; (**C**) Base peak map of RMLG negative ion model.

equal volumes of pure water intragastrically. One hour after the last dose, blood samples were collected and centrifuged at 4 °C at 12000 rpm for 15 min, then the supernatant was collected. The serum was then heat-inactivated at 56 °C for 30 min and filtered to remove bacteria. The RMLG drug-containing serum was diluted with 10% fetal bovine serum to final concentrations of 2.5, 5, and 10% to create low, medium, and high doses of RMLG drug-containing serum, respectively.

When the cells had grown to 70–80% confluence, they were divided into a normal medium (control) group, blank serum (blank) group, RMLG drug-containing serum low-dose (RMLG-L) group, RMLG drug-containing serum medium-dose (RMLG-M) group, and RMLG drug-containing serum high-dose (RMLG-H) group, with three replicates in each group. A colony formation assay was used to determine the concentration of RMLG drug-containing serum administered.

The HCECs used in the subsequent experiments were divided into six groups: the control group, model group, RMLG drug-containing serum high-dose (RMLG-H) group, NLRP3 inflammasome silencing (NLRP3-siRNA) group, NLRP3 inflammasome activator (nigericin) group, and negative control siRNA (NC-siRNA) group, with three replicates in each group. Cells were treated with 0.01% BAC for 6 h in all groups except the control group. The RMLG-H group was given 10% RMLG drug-containing serum for 3 h, and the nigericin group was treated with a dose of 10 μM nigericin for 30 min. Cells in the NLRP3-siRNA and NC-siRNA groups were transfected and treated with BAC, respectively.

Detection Indicators and Methods
Corneal Fluorescein Staining (CFS)
A fluorescein ophthalmologic test strip (Jingming New Technological Development Co., Ltd. Tianjin, China) was moistened with normal saline, and the conjunctiva of the lower fornix was gently touched. Corneal fluorescein staining

was performed under cobalt blue light using a slit-lamp microscope (Sunkingdom Medical Instrument Co., Ltd. Chongqing, China). The cornea was evenly divided into four quadrants, and the sodium fluorescein staining in each quadrant was recorded as follows: 0 points indicated no staining, 1 point indicated <30 dots of coloring, 2 points indicated >30 spots of coloring but no fusion, and 3 points indicated >30 spots of coloring with block dyeing or filamentous matter. The maximum possible score was 12.[33]

Tear Break-Up Time (TBUT)
The corneas of the rats were stained with fluorescein and observed under cobalt blue light using a slit-lamp microscope in an unventilated environment. After blinking, the eyes of the rats were kept open, and the time interval for the first dry spot to appear on the tear film surface was measured. The average value was calculated from three measurements per eye.[34]

Phenol Red Tear Test (PRTT)
The PRTT method was used to detect tear flow in each group. Phenol red cotton thread (Jingming New Technological Development Co., Ltd. Tianjin, China) was removed using micropliers, and the lower eyelid of the rats was slightly pulled down. The top of the line was placed 1 mm on the conjunctiva of the eyelid at approximately one-third of the distance from the outer canthus of the lower eyelid, and the eyes were closed for 20s. Using a scale, we measured the length of the cotton thread from the yellow to the red area. The measurements were repeated three times for each eye, and the values obtained were averaged.[35]

Histopathological Examination
The pathological changes of corneal tissue in each group were observed using hematoxylin and eosin (H&E) staining. The corneas were fixed in a 4% paraformaldehyde solution for 1 d, dehydrated with gradient alcohol, made transparent with xylene, and embedded in paraffin. The paraffin-fixed corneal tissue was sectioned, then sliced at a thickness of 4 μm, and stained with H&E. Finally, the sections were sealed with a neutral resin. The samples were observed and photographed under a light microscope.

Terminal Deoxynucleotidyl Transferase-Mediated dUTP Nick-End Labeling (TUNEL)
The corneal tissue was fixed in 4% paraformaldehyde, embedded in paraffin, sectioned, and prepared for TUNEL staining. After baking, dewaxing, soaking in distilled water, PBS washing, nuclear staining, and other steps, the slides were sealed with 90% glycerol. Corneal cell injury in each group was observed under a microscope.

Transmission Electron Microscopy (TEM)
Ultrastructural changes in the corneal tissues were observed using TEM. Small samples of corneal tissue were fixed in an electron microscope fixative at 4°C for 2 h and then washed twice with PBS. Samples were fixed with 1% osmic acid for 1 h, dehydrated with acetone, and embedded in epoxide resin. Ultrathin sections were prepared, stained with uranyl acetate and lead citrate, and observed using TEM.

Immunofluorescence Detection
Paraffin sections of the corneal tissue were roasted in an oven at 60 °C for 20 min and dewaxed with xylene, then hydrated with gradient ethanol and repaired with antigen. After blocking with 5% bovine serum albumin at room temperature for 20 min, the sections were incubated overnight at 4 °C with primary antibodies (NLRP3 diluted to 1:200, GSDMD diluted to 1:300). Subsequently, the sections were incubated with anti-rabbit (1:500) and anti-mouse (1:500) secondary antibodies for 30 min and DAPI for 2 min at a room temperature of 25 °C. Finally, a fluorescence microscope (Mingmei Photoelectric Technology Co., Ltd., Guangzhou, China) was used to observe the protein expression in the samples, and semi-quantitative analysis was performed using the ImageJ software (National Institutes of Health, USA).

Western Blotting Analysis
Fresh corneal tissue samples and HCEC were placed in pre-cooled RIPA lysis (containing 1% protease inhibitor), fully ground with a tissue grinder, and then centrifuged at 4 °C at 12000 rpm for 15 min. The protein in the supernatant was quantified using the BCA kit. The protein samples were thoroughly mixed with SDS-PAGE sample buffer and denatured in a boiling water bath for 10 min. Proteins with different molecular weights were separated using 8–15% SDS

polyacrylamide gel electrophoresis and membrane electrotransfer. The film was sealed with 5% skim milk powder at room temperature for 1 h, and then incubated with primary antibodies at 4 °C overnight. After incubation with secondary antibody at room temperature for 1 h, the bands were detected using a chemiluminescence detection system. Band densities were examined using the ImageJ software. Values are expressed as the band intensity normalized to that of β-actin.

Colony Formation

Cells from each group were seeded in 6-well plates and cultured for 14 d. Subsequently, cells were fixed with 4% paraformaldehyde for 15 min and stained with 0.1% crystal violet for 10 min. The colonies were photographed, and the ImageJ software was used to count the number of colonies. Relative colony numbers = clone numbers/average clone number of the control group.[36]

Annexin V-PI Staining

After trypsin digestion, cells in each group were centrifuged and resuspended. The cell suspension was collected, and 5 μL of Annexin V FITC and 10 μL of propidium iodide solution were added, followed by incubation for 15 min in the dark. The results were analyzed using flow cytometry.

Statistical Analysis

Statistical analyses were performed using GraphPad Prism version 8.3.0 (GraphPad Software, Inc. San Diego, USA). The data were expressed as the mean ± standard error. Student's *t*-test or one-way analysis of variance was used to compare differences between two or more groups. Statistical significance was set at P-values < 0.05.

Results

Identification of the Metabolites in RMLG

The metabolites of RMLG were analyzed using UHPLC-MS/MS. We conducted detection in positive (ESI+) and negative ionization (ESI-) modes and obtained representative total LC-MS ion current chromatograms (Figure 1B and C). According to the results, 360 metabolites were identified in RMLG, with 298 identified in positive ion mode and 142 in negative ion mode. Eighty metabolites were detected in both ion modes. The identified metabolites included 65 amino acids and their derivatives, 57 fatty acids, 39 carboxylic acids and their derivatives, 37 organo-oxygen compounds, and 35 flavonoid O-glycosides (Supplementary Material 1).
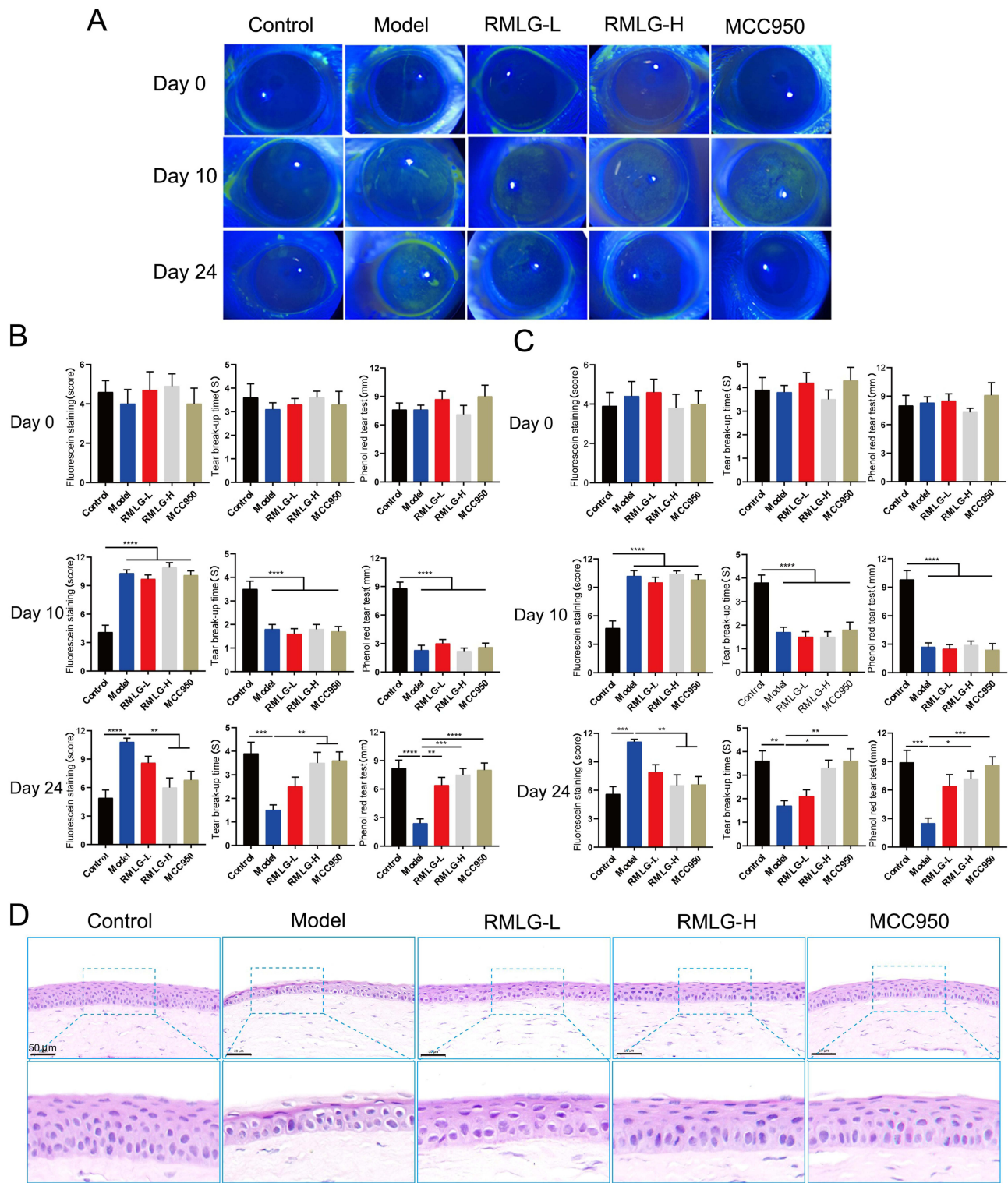
RMLG Improves DE Signs and Relieves the Histopathological Damage of the Cornea in DE Rats

Ten days after Scop injection, the corneas of the DE rats were susceptible to varying degrees of impairment (Figure 2A). Hence, to investigate the effects of RMLG on the symptoms of DE in rats, we conducted a series of experiments, including CFS, TBUT, and PRTT. Our observations suggest that RMLG treatment significantly alleviated ocular surface signs in experimental DE model rats, which was manifested as diminished corneal fluorescence staining, prolonged tear film break-up time, and increased tear secretion (Figure 2B and C).

To evaluate the effect of RMLG on corneal tissue damage induced by Scop, H&E staining was used to observe corneal epithelial injury in DE rats (Figure 2D). The control group showed a complete corneal tissue structure with uniformly sized and tightly arranged cells. The collagen fibers in the stromal layer were consistent. In contrast, the DE group displayed irregularly shaped corneal epithelial cells, partially detached corneal tissue structure, a thin epithelial cell layer, reduced cell density, and cytoplasmic vacuolization. RMLG treatment ameliorated corneal histopathological changes in DE rats.
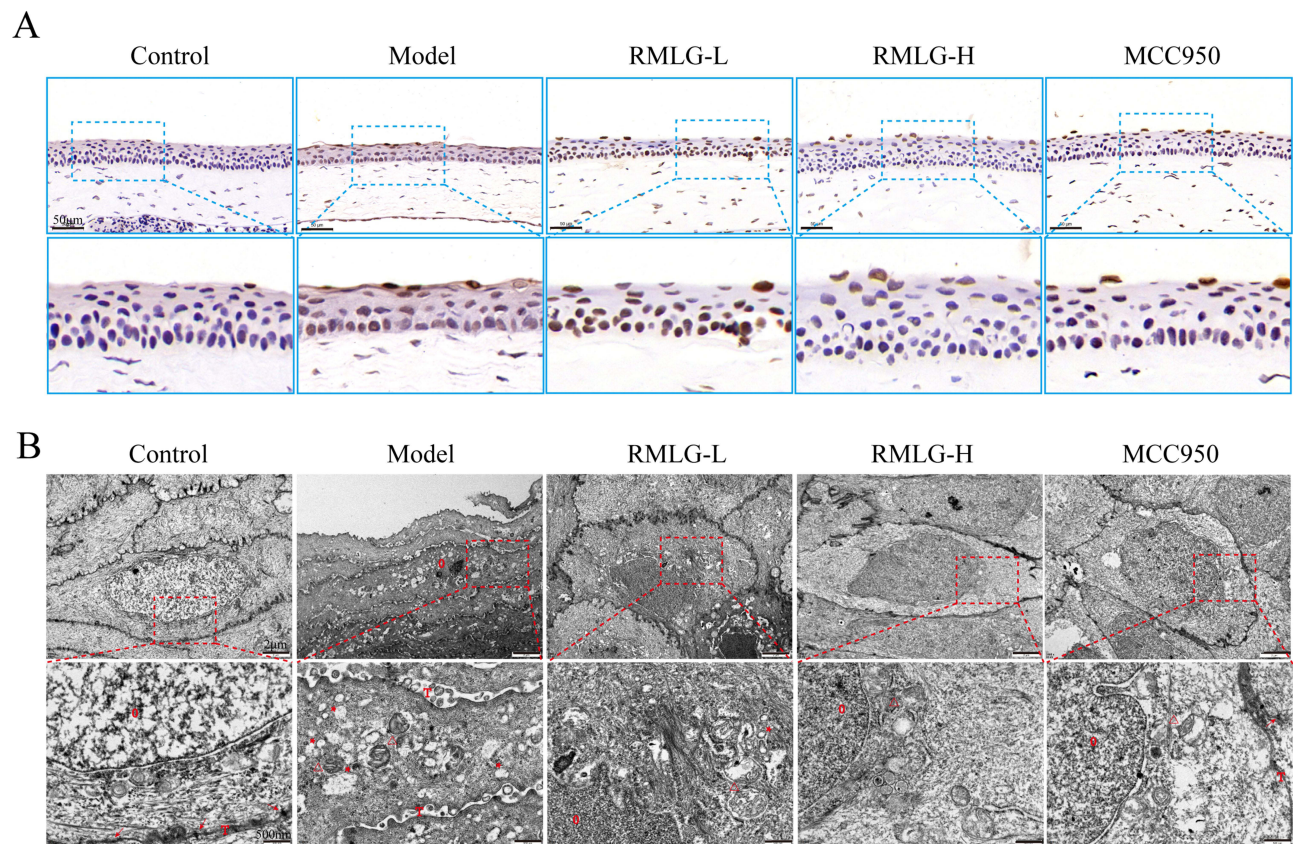
RMLG Alleviated Corneal Epithelial Cell Damage and Improved the Ultrastructure of Corneal Tissue in DE Rats

TUNEL staining was used to observe corneal epithelial cell injury in each group (Figure 3A). Our results showed that corneal epithelial cell injury was significant in the Scop-induced DE model rats, with damaged cells displaying brown-

Figure 2 RMLG improves dry eye (DE) signs and relieves histopathological damage to the cornea in rats with DE. (**A**) Representative image of corneal fluorescein staining in each group of rats at different times. (**B**) Effects of RMLG on the CFS, TBUT, and PRTT in the right and (**C**) left rat eyes with DE (n=10). (**D**) Representative images of histological changes in five groups of rats (H&E staining, magnification 200 ×, Scale bar:50μm). *P < 0.05, **P < 0.01, ***P < 0.001 and ****P < 0.0001.

Figure 3 RMLG alleviated corneal epithelial cell damage and improved ultrastructural corneal tissue features in rats with DE. (**A**) Images of the injury to the corneal epithelial cells in each group (TUNEL, magnification 200 ×, Scale bar: 50 μm.); (**B**) Ultrastructural changes in corneal epithelial cells in rats. 0: Cell nucleus; (T) cell membrane; ▲: Organelles; *: vacuolar cytoplasm; →: desmosomal (TEM, magnification 2500× and 10000×, Scale bar: 2 μm and 500 nm).

yellow nuclear staining. After RMLG treatment, the number of damaged cells was significantly reduced, and cell damage was alleviated.

Ultrastructural changes in rat corneal epithelial cells were observed using TEM (Figure 3B). In the control group, the cell structure was intact, with normal organelle morphology and a complete and continuous cell membrane structure. In the corneal epithelium of rats in the DE model, the number of pyroptotic cells increased significantly, as evidenced by the peripheral concentration of nuclear chromatin, nuclear collapse, edema expansion of endoplasmic reticulum and mitochondria, vacuolar cytoplasm, discontinuity of cell membrane, cell swelling, and reduced desmosomal junctions between cells. Compared to the DE group, the RMLG and MCC950 groups showed much less pathological damage.

RMLG Treatment Attenuated the Protein Expression of the NLRP3/GSDMD Signaling Pathway in DE Rats

To elucidate the potential molecular mechanisms of RMLG in DE, we investigated NLRP3/GSDMD pathway expression using immunofluorescence and Western blotting analyses (Figure 4). The immunofluorescence results showed that the expression of NLRP3 and GSDMD in the cornea was significantly enhanced in the model group. Following treatment, the levels of these factors significantly decreased in the RMLG and MCC950 groups (Figure 4A and B). The Western blot analysis revealed that Scop significantly increased NLRP3, GSDMD, ASC, Pro-caspase-1, Cleaved caspase-1, IL-18, IL-1β, and TNF-α protein expression in the cornea tissue samples from DE rats compared to those observed in the control samples and RMLG treatment reversed these changes (Figure 4C and D). Our findings demonstrate that RMLG significantly reduces NLRP3/GSDMD-mediated pyroptosis pathway-associated protein upregulation in DE rats.
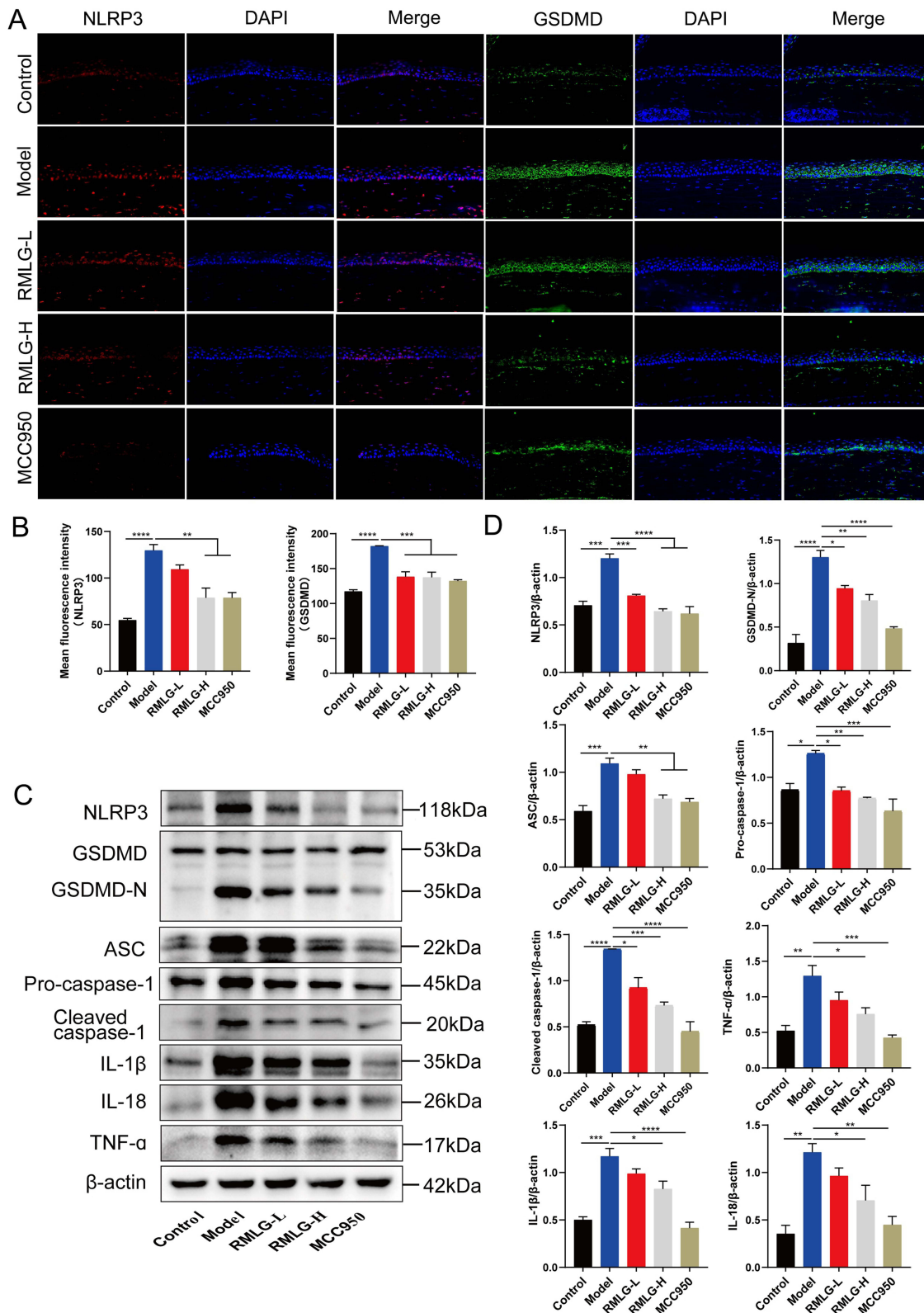
Figure 4 RMLG treatment attenuates the expression of the NLRP3/GSDMD signaling pathway in DE rats. (**A**) Immunofluorescence and (**B**) semi-quantitative analysis (mean intensity) of NLRP3 and GSDMD expression in the cornea. (**C**) Western blot bands of NLRP3, GSDMD, Pro-caspase-1, Cleaved caspase-1, ASC, IL-1β, IL-18, TNF-α, and β-actin. (**D**) Western blot data were quantified using densitometric analysis and normalized to β-actin (n=3). *P < 0.05, **P < 0.01, ***P < 0.001 and ****P < 0.0001.

RMLG Reduce Inflammation and Prevents Cell Pyroptosis in HCECs

To simulate the DE inflammatory model in HCECs, we treated the cells with gradient concentrations of BAC. HCECs were incubated with various concentrations of BAC (0.0005, 0.001, 0.005, 0.01, 0.05, and 0.1%) for 6 h, and CCK-8 assays were performed. BAC inhibited HCEC proliferation in a dose-dependent manner (Figure 5A). After 6 h of exposure, the IC50 value of BAC in HCECs was 0.001%. For subsequent analyses, we chose a 0.01% BAC concentration for HCECs. To investigate the effect of RMLG on HCEC proliferation, we conducted a colony formation assay. HCECs were treated with various concentrations of RMLG (2.5, 5, and 10%) for 3 h, stimulated with 0.01% BAC for 6 h, and subjected to a colony formation assay. The results suggested that blank serum treatment did not induce cell death, BAC treatment significantly inhibited cell viability, and the RMLG at medium and high doses notably enhanced HCEC growth in vitro (Figure 5B and C).

To verify at the cellular level that RMLG can reduce HCEC inflammation by inhibiting the NLRP3/GSDMD-mediated pyroptosis pathway, we treated the cells with NLRP3-siRNA and the NLRP3 activator nigericin. Western blotting was performed to verify the silencing effect of the target gene NLRP3. Western blotting results showed that NLRP3 was expressed at low levels after transfection (Figure 5D and E). During pyroptosis, GSDMD-N binds to lipids in the plasma membrane to form large oligomeric pores, releasing cell contents and revealing stained dead cells as determined by propidium iodide staining (Figure 5F and G). Cells treated with BAC alone and NLRP3 activator showed increased pyroptosis; RMLG and NLRP3 siRNA effectively interrupted all of these events. At the same time, the Western blotting experiment showed that RMLG treatment could alleviate the generation of NLRP3, ASC, Pro-caspase -1, and Cleaved caspase-1 protein and effectively reduce the release of IL-1β, IL18, and TNF-α inflammatory factors (Figure 6A and B). All this evidence suggests that NLRP3 inflammasomes play a key role in HCEC pyroptosis and demonstrates that RMLG alleviates HCEC inflammation by inhibiting the NLRP3-mediated pyroptosis pathway. Both in-vivo and in-vitro experimental results suggest that the NLRP3/GSDMD-mediated pyroptosis pathway underlies ocular surface inflammation in DE. Additionally, our findings indicate that RMLG exerts anti-inflammatory effects by inhibiting the NLRP3/GSDMD pathway.

Discussion

Tear hyperosmolarity and tear instability are core drivers of DE, as they damage the ocular surface directly and by initiating inflammation.[3] Therefore, Inflammatory damage to the ocular surface plays an important role in the development of DE.[7,37] Activation of the NLRP3 inflammasome is a key driver of ocular surface inflammatory injury in DE.[9] Pathogen- or damage-associated molecular patterns can activate the cytoplasmic innate immune signaling receptor NLRP3, leading to caspase 1-mediated activation of the IL-1β family of cytokines, which contributes to the assembly of inflammasomes and ultimately induces inflammatory, lytic cell death.[38] Herein, rats with scop-induced DE exhibited reduced tear production, loss of tear film homeostasis, and ocular surface damage (Figure 2A−C) along with histopathological changes in the cornea (Figure 2D) and damage to corneal epithelial cells (Figure 3A), suggesting the development of DE, which is consistent with previous studies.[39]

Additionally, our in-vitro experiments confirmed that BAC induction caused varying degrees of damage to HCECs (Figure 5A). Studies have shown that DE can be effectively prevented and treated by inhibiting NLRP3-mediated cytokine production. Ren et al[40] found that miR-223 significantly helps treat DE by inhibiting NLRP3 translation, thereby reducing NLRP3 inflammasome activity, oxidative stress, and inflammatory response. In this study, we used several indicators to demonstrate the role of RMLG in the treatment of DE by reducing inflammatory damage to the ocular surface. The results showed that RMLG significantly reduced corneal tissue damage, improved tear film stability, and increased tear secretion in scop-induced DE rats (Figure 2) while enhancing BAC-induced cell viability of HCECs (Figure 5), inhibiting the expression of the NLRP3 inflammasome, and reducing the expression of inflammatory cytokines such as IL-1β, IL-18, and TNF-α (Figure 6), thus demonstrating its protective effect. These findings suggest that RMLG has anti-inflammatory effects and can attenuate DE by inhibiting inflammation-related injuries.

Pyroptosis, a regulated form of cell death dependent on the gasdermin protein family, also contributes to DE pathogenesis and acts synergistically with the NLRP3 inflammasome.[8,41] In the canonical pyroptotic pathway, pathogens or other stimuli
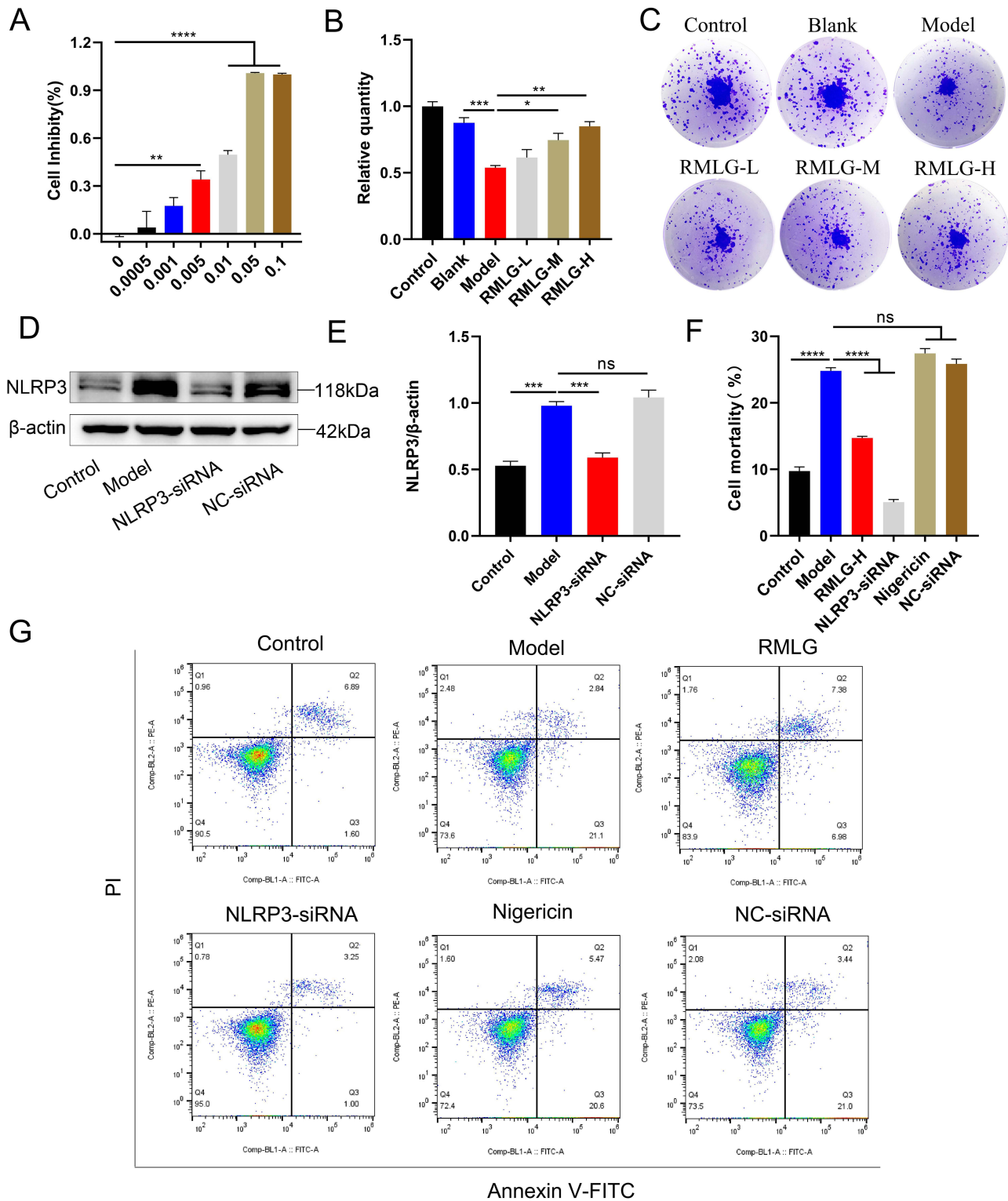
Figure 5 RMLG enhances the viability and reduces pyroptosis levels in HCECs. (**A**) The CCK-8 assay showed that BAC inhibited HCEC viability in a dose-dependent manner. (**B** and **C**) Colony formation assays showed that RMLG significantly inhibited BAC-induced cell death in a dose-dependent manner. (**D**) Western blot bands for NLRP3 and β-actin. (**E**) Western blot data were quantified using densitometric analysis and normalized to β-actin (n=3). (**F**) Flow cytometry quantification displayed active cells as the pyroptotic population. *$P < 0.05$, **$P < 0.01$, ***$P < 0.001$ and ****$P < 0.0001$. (**G**) Representative flow cytometry dot plots.

10780

Journal of Inflammation Research 2024:17
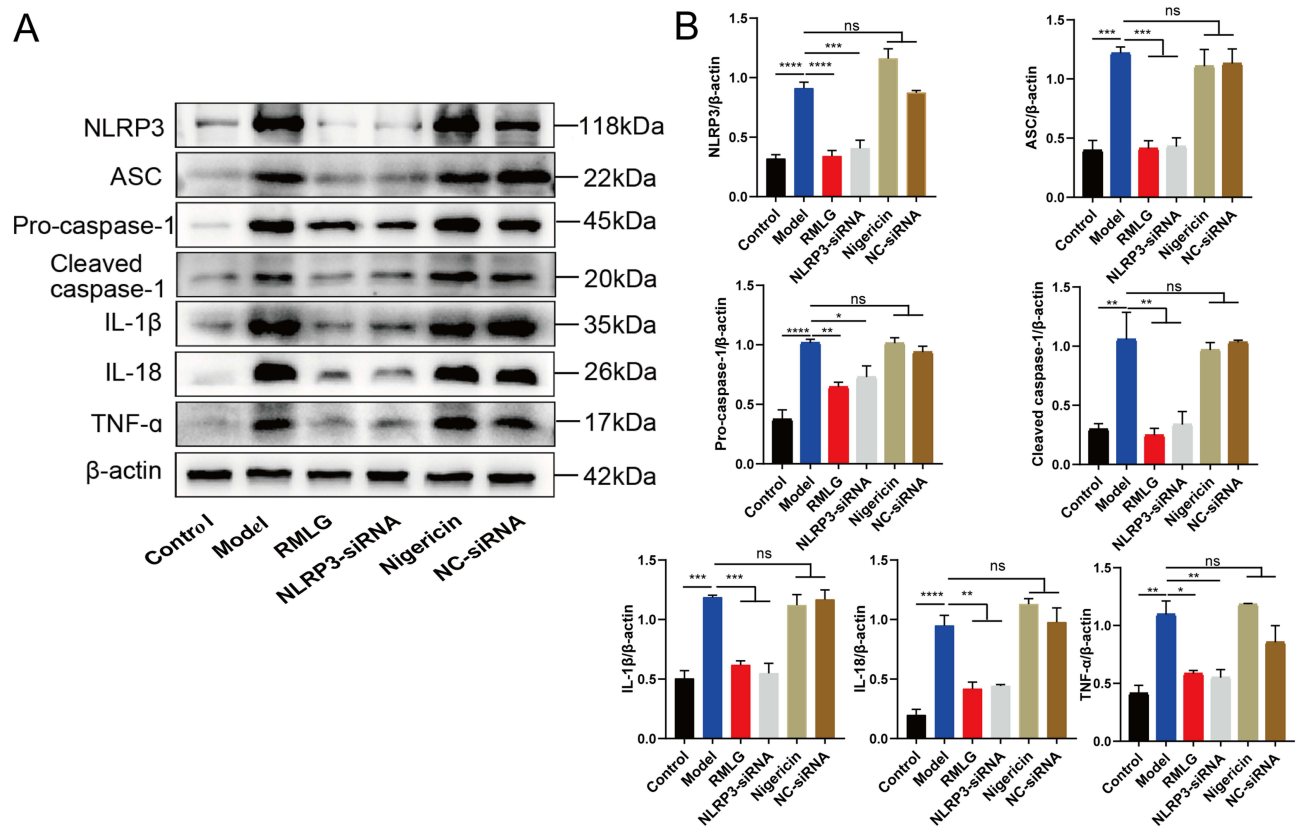
Figure 6 RMLG reduce inflammation in HCECs. (**A**) Western blot bands of NLRP3, Pro-caspase-1, Cleaved caspase-1, ASC, IL-1β, IL-18, TNF-α, and β-actin. (**B**) Western blot data were quantified using densitometric analysis and normalized to β-actin (n=3). *P < 0.05, **P < 0.01, ***P < 0.001 and ****P < 0.0001.

trigger NLRP3 inflammasome aggregation, leading to caspase-1 activation and GSDMD cleavage. The N-terminal fragment of GSDMD (GSDMD-N) generates pores in the phospholipids of the plasma membrane, resulting in cell lysis and consequent cell death.[18] Blocking the NLRP3 and GSDMD pathways has been shown to effectively treat DE.[42,43] We observed extensive GSDMD expression in the corneal tissues of scopolamine-induced DE rats using immunofluorescence and Western blotting (Figure 4A and B). DE led to the onset of cellular pyroptosis, which was also confirmed by the TME ultrastructure (Figure 3B). Therefore, we sought to determine the role of NLRP3/GSDMD-mediated pyroptosis in scopolamine-induced corneal epithelial cell damage and BAC-induced inflammatory injury in HCECs and its protection by RMLG. We treated DE rats with NLRP3 inhibitors and used siRNA silencing of NLRP3 and nigericin activation of NLRP3 in vitro. NLRP3 activation (nigericin) enhanced pyroptosis, while inhibition (MCC950) or silencing (NLRP3-siRNA) decreased it. Additionally, RMLG significantly reduced the relative expression of NLRP3, GSDMD, ASC, Pro-caspase-1, and Cleaved caspase-1 proteins, thereby attenuating the inflammatory responses induced by the downstream pro-inflammatory mediators IL-1β, IL-18, and TNF-α. Our data suggest that RMLG may exert its therapeutic effect on DE by regulating the NLRP3/GSDMD-mediated pyroptosis pathway (Figure 7).

However, this study had some limitations. Firstly, RMLG has multiple targets and pathways, but we only investigated its regulatory role in the NLRP3/GSDMD signaling pathway and proteins or pathways that mediate upstream inflammation. More investigations are needed to further reveal the specific molecular mechanisms of RMLG in treating ocular surface inflammation in DE. Secondly, we tested only indices of the corneal tissue. In future studies, we will evaluate the effect of RMLG in the treatment of DE by examining other ocular surface tissues, such as the conjunctiva and the lacrimal gland.
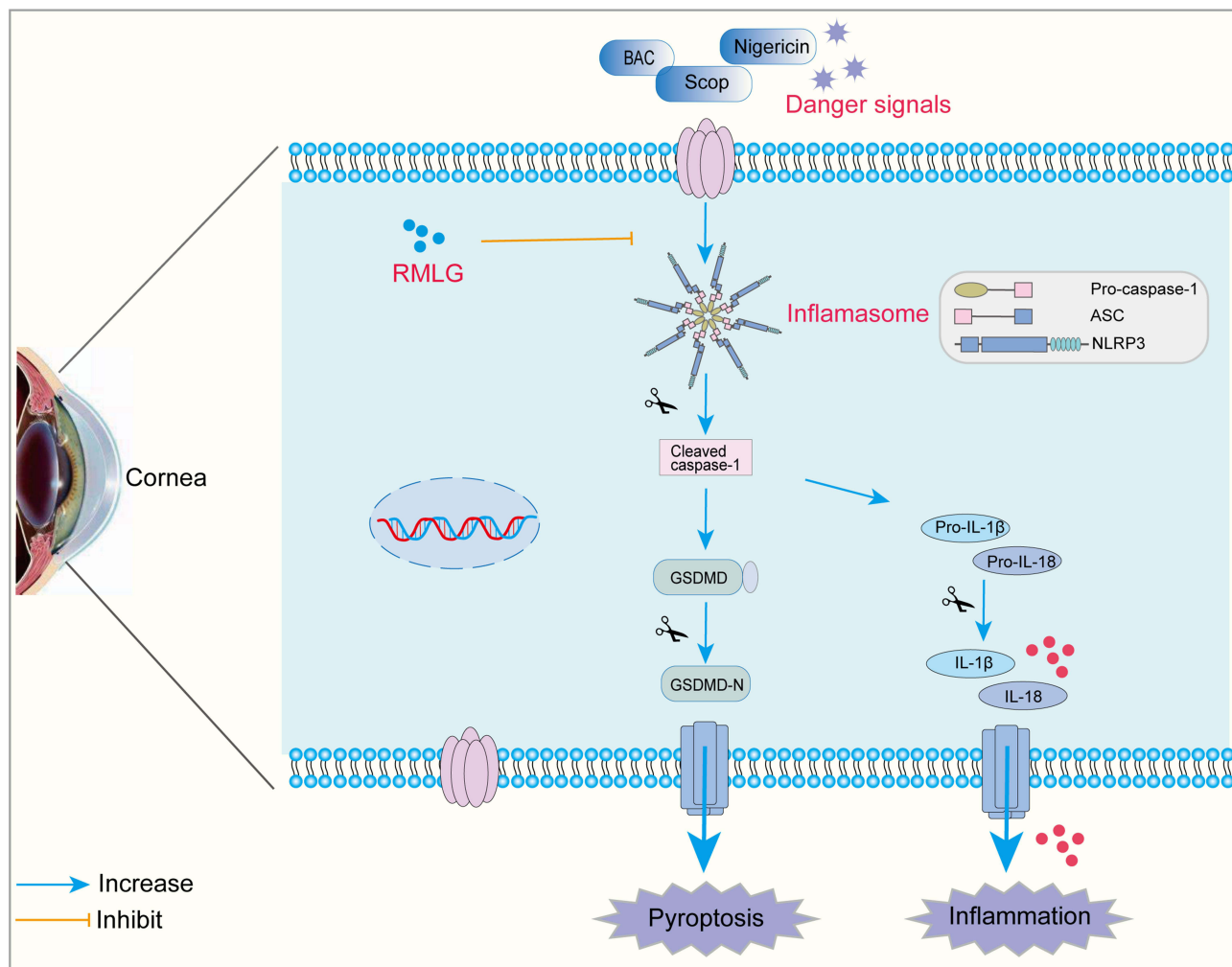
Figure 7 Schematic diagram of the mechanism of RMLG inhibiting NLRP3/GSDMD-mediated pyroptosis pathway.

Conclusion

In conclusion, this study investigated the therapeutic effects of RMLG on ocular surface inflammation in DE, both in vitro and in vivo, and explored its potential underlying mechanisms. Our findings indicate that RMLG inhibited pyroptosis, reduced pro-inflammatory factor expression levels, alleviated ocular surface inflammation, and ameliorated DE symptoms, the mechanism of action of RMLG is related to the inhibition of the activation of NLRP3/GSDMD-mediated pyroptosis pathway. These insights enhance our understanding of DE pathogenesis and suggest that RMLG could be a promising therapeutic option for the prevention and management of DE.

Data Sharing Statement

The data generated in the study are included in the article/supplementary material, and further inquiries can be directed to the corresponding authors.

Author Contributions

All authors made a significant contribution to the work reported, whether that is in the conception, study design, execution, acquisition of data, analysis and interpretation, or in all these areas; took part in drafting, revising or critically reviewing the article; gave final approval of the version to be published; have agreed on the journal to which the article has been submitted; and agree to be accountable for all aspects of the work.

10782

Journal of Inflammation Research 2024:17

Funding

Disclosure

The authors declare that the research was conducted in the absence of any commercial or financial relationships that could be construed as a potential conflict of interest.

References

1. Craig JP, Nichols KK, Akpek EK, et al. TFOS DEWS II Definition and Classification Report. *Ocul Surf*. 2017;15(3):276–283. doi:10.1016/j. jtos.2017.05.008
2. Stapleton F, Alves M, Bunya VY, et al. TFOS DEWS II Epidemiology Report. *Ocul Surf*. 2017;15(3):334–365. doi:10.1016/j.jtos.2017.05.003
3. Bron AJ, de Paiva CS, Chauhan SK, et al. TFOS DEWS II pathophysiology report. *Ocul Surf*. 2017;15(3):438–510. doi:10.1016/j.jtos.2017.05.011
4. Alves M, Asbell P, Dogru M, et al. TFOS Lifestyle Report: impact of environmental conditions on the ocular surface. *Ocul Surf*. 2023;29:1–52. doi:10.1016/j.jtos.2023.04.007
5. Jones L, Downie LE, Korb D, et al. TFOS DEWS II Management and Therapy Report. *Ocul Surf*. 2017;15(3):575–628. doi:10.1016/j. jtos.2017.05.006
6. Li S, Lu ZY, Huang Y, et al. Anti-Oxidative and Anti-Inflammatory Micelles: break the Dry Eye Vicious Cycle. *Adv Sci*. 2022;9(17). doi:10.1002/advs.202200435
7. Zemanova M. DRY EYE DISEASE. A REVIEW. *Cesk Slov Oftalmol*. 2021;77(3):107–119. doi:10.31348/2020/29
8. Zhang Y, Jiao Y, Li X, et al. Pyroptosis: a New Insight Into Eye Disease Therapy. *Front Pharmacol*. 2021;12. doi:10.3389/fphar.2021.797110.
9. Zhuang D, Misra SL, Mugisho OO, Rupenthal ID, Craig JP. NLRP3 Inflammasome as a Potential Therapeutic Target in Dry Eye Disease. *Int J Mol Sci*. 2023;24(13):10866. doi:10.3390/ijms241310866
10. Sharif H, Wang L, Wang WL, et al. Structural mechanism for NEK7-licensed activation of NLRP3 inflammasome. *Nature*. 2019;570(7761):338. doi:10.1038/s41586-019-1295-z
11. Zychlinsky A, Prevost MC, Sansonetti PJ. Shigella flexneri induces apoptosis in infected macrophages. *Nature*. 1992;358:6382):167–169. doi:10.1038/358167a0
12. Li Q, Shi NX, Cai C, et al. The Role of Mitochondria in Pyroptosis (Publication with Expression of Concern. *Front Cell Dev Biol*. 2021;8 doi:10.3389/fcell.2020.630771.
13. Kovacs SB, Miao EA. Gasdermins: effectors of Pyroptosis. *Trends Cell Biol*. 2017;27(9):673–684. doi:10.1016/j.tcb.2017.05.005
14. Xu S, Liu XT, Liu XT, et al. Wedelolactone ameliorates Pseudomonas aeruginosa-induced inflammation and corneal injury by suppressing caspase-4/5/11/GSDMD-mediated non-canonical pyroptosis. *Exp Eye Res*. 2021;211. doi:10.1016/j.exer.2021.108750.
15. Meng CR, Gu CF, He S, et al. Pyroptosis in the Retinal Neurovascular Unit: new Insights Into Diabetic Retinopathy. *Front Immunol*. 2021;12. doi:10.3389/fimmu.2021.763092.
16. Sun Y, Li F, Liu Y, et al. Targeting inflammasomes and pyroptosis in retinal diseases-molecular mechanisms and future perspectives. *Prog Retin Eye Res*. 2024;101:101263. doi:10.1016/j.preteyeres.2024.101263
17. Han Y, Zhang Y, Yuan KL, Wu YY, Jin XM, Huang XD. Hyperosmolarity promotes macrophage pyroptosis by driving the glycolytic reprogramming of corneal epithelial cells in dry eye disease. *Front Med*. 2023;17(4):781–795. doi:10.1007/s11684-023-0986-x
18. Scarpellini C, Llorca AR, Lanthier C, Klejborowska G, Augustyns K. The Potential Role of Regulated Cell Death in Dry Eye Diseases and Ocular Surface Dysfunction. *Int J Mol Sci*. 2023;24(1):731. doi:10.3390/ijms24010731
19. Yang X, Zuo X, Zeng H, et al. IFN-? Facilitates Corneal Epithelial Cell Pyroptosis Through the JAK2/STAT1 Pathway in Dry Eye. *Invest Ophthalmol Vis Sci*. 2023;64(3):34. doi:10.1167/iovs.64.3.34
20. Liao K, Zeng H, Yang X, He DL, Wang BW, Yuan J. KCNK5 Regulating Potassium Efflux and Inducing Pyroptosis in Corneal Epithelial Cells Through TNFSF10-Mediated Autophagy in Dry Eye. *Invest Ophthalmol Vis Sci*. 2024;65(1):34. doi:10.1167/iovs.65.1.34
21. Li XJ, Chen C, Chen Y, et al. Oridonin ameliorates ocular surface inflammatory responses by inhibiting the NLRP3/caspase-1/GSDMD pyroptosis pathway in dry eye. *Exp Eye Res*. 2024;245. doi:10.1016/j.exer.2024.109955
22. Yang MY, Hu ZP, Yue RS, Yang LJ, Zhang BX, Chen Y. The Efficacy and Safety of Qiming Granule for Dry Eye Disease: a Systematic Review and Meta-Analysis. *Front Pharmacol*. 2020;11. doi:10.3389/fphar.2020.00580
23. Yang CC, Chien JY, Chou YY, Ciou JW, Huang SP. The Effects of Lycium chinense, Cuscuta chinensis, Senna tora, Ophiopogon japonicus, and Dendrobium nobile Decoction on a Dry Eye Mouse Model. *Medicina*. 2022;58(8). doi:10.3390/medicina58081134
24. Xu J, Chen ST, Hao XF, et al. Traditional Chinese medicine Xiaosheng Powder for dry eye disease A protocol for systematic review and meta analysis. *Medicine*. 2020;99(35):e23466. doi:10.1097/MD.0000000000023466
25. Xu W, Liu X, Gao W. Influence of Runmuling Granules on Morphology and Apoptosis -related Factors of Lacrimal Gland in Aqueous Tear Deficiency Dry Eye Model Rabbits. *Tradit Chin Drug Res Clin Pharm*. 2015;26(4):425–430.
26. Song J, Liu X, Qi X, et al. Investigation on Treatment of Xerophthalmia Induced by Benzalkonium Chloride with Runmuling Eye-Drops and Its Underlying Mechanism. *J Nanjing Univ Traditional Chin Med*. 2023;39(1):70–78.
27. Zhang C, Li K, Yang Z, Wang Y, Si H. The Effect of the Aqueous Extract of Bidens Pilosa L. on Androgen Deficiency Dry Eye in Rats. *Cell Physiol Biochem*. 2016;39(1):266–277. doi:10.1159/000445622
28. Li YQ, Sun XQ, Liu XN, et al. P2X7R-NEK7-NLRP3 Inflammasome Activation: a Novel Therapeutic Pathway of Qishen Granule in the Treatment of Acute Myocardial Ischemia. *J Inflamm Res*. 2022;15:5309–5326. doi:10.2147/JIR.S373962

29. Chaudhari P, Satarker S, Thomas R, et al. Rodent models for dry eye syndrome: standardization using benzalkonium chloride and scopolamine hydrobromide. *Life Sci.* 2023;317. doi:10.1016/j.lfs.2023.121463

30. Liu P, Jiang PF, Yu YF, et al. Modified Danzhi Xiaoyao Powder (MDXP) improves the corneal damage in dry eye disease (DED) mice through phagocytosis. *J Ethnopharmacol.* 2024;321. doi:10.1016/j.jep.2023.117544

31. Zhou JJ, Zhang C, Fang X, Zhang NX, Zhang XX, Zhu ZQ. Activation of autophagy inhibits the activation of NLRP3 inflammasome and alleviates sevoflurane-induced cognitive dysfunction in elderly rats. *BMC Neurosci.* 2023;24(1). doi:10.1186/s12868-023-00777-5

32. Zhang R, Park M, Richardson A, et al. Dose-dependent benzalkonium chloride toxicity imparts ocular surface epithelial changes with features of dry eye disease. *Ocul Surf.* 2020;18(1):158–169. doi:10.1016/j.jtos.2019.11.006

33. Wu HM, Lin LF, Du XY, et al. Study on the potential effective ingredients of Xiaosheng prescription for dry eye disease. *Biomed Pharmacother.* 2020;127. doi:10.1016/j.biopha.2020.110051

34. Shanmugham V, Subban R. Capsanthin from Capsicum annum fruits exerts anti-glaucoma, antioxidant, anti-inflammatory activity, and corneal pro-inflammatory cytokine gene expression in a benzalkonium chloride-induced rat dry eye model. *J Food Biochem.* 2022;46(10):e14352. doi:10.1111/jfbc.14352

35. Li H, Wei F, Li SW, Yan L, Lu PR. The effect of sinomenine eye drops on experimental dry eye in mice. *Cutan Ocul Toxicol.* 2020;39(4):389–395. doi:10.1080/15569527.2020.1840580

36. Yang WC, Wang YX, Huang YZ, et al. 4-Octyl itaconate inhibits aerobic glycolysis by targeting GAPDH to promote cuproptosis in colorectal cancer. *Biomed Pharmacother.* 2023;9. doi:10.1016/j.biopha.2023.114301

37. Yu LF, Yu CJ, Dong H, et al. Recent Developments About the Pathogenesis of Dry Eye Disease: based on Immune Inflammatory Mechanisms. *Front Pharmacol.* 2021;12.

38. Mangan MSJ, Olhava EJ, Roush WR, Seidel HM, Glick GD, Latz E. Targeting the NLRP3 inflammasome in inflammatory diseases. *Nat Rev Drug Discov.* 2018;17(8):588–606. doi:10.1038/nrd.2018.97

39. Yu ZY, Yazdanpanah G, Alam J, de Paiva CS, Pflugfelder S, de Paiva CS. Induction of Innate Inflammatory Pathways in the Corneal Epithelium in the Desiccating Stress Dry Eye Model. *Invest Ophthalmol Vis Sci.* 2023;64(4):8. doi:10.1167/iovs.64.4.8

40. Ren YP, Feng JY, Lin Y, et al. MiR-223 inhibits hyperosmolarity-induced inflammation through downregulating NLRP3 activation in human corneal epithelial cells and dry eye patients. *Exp Eye Res.* 2022;220.

41. Galluzzi L, Vitale I, Aaronson SA, et al. Molecular mechanisms of cell death: recommendations of the Nomenclature Committee on Cell Death 2018. *Cell Death Differ.* 2018;25(3):486–541. doi:10.1038/s41418-017-0012-4

42. Zhang J, Dai YQ, Yang YJ, Xu JJ. Calcitriol Alleviates Hyperosmotic Stress-Induced Corneal Epithelial Cell Damage via Inhibiting the NLRP3-ASC-Caspase-1-GSDMD Pyroptosis Pathway in Dry Eye Disease. *J Inflamm Res.* 2021;14:2955–2962. doi:10.2147/JIR.S310116

43. Lou Q, Pan L, Xiang SJ, et al. Suppression of NLRP3/Caspase-1/GSDMD Mediated Corneal Epithelium Pyroptosis Using Melatonin-Loaded Liposomes to Inhibit Benzalkonium Chloride-Induced Dry Eye Disease. *Int J Nanomed.* 2023;18:2447–2463. doi:10.2147/IJN.S403337